Mixed Oxide Surfaces: Ultrathin Films of $Ca_xMg_{(1-x)}O$

M. J. Iedema,*,† N. Kizhakevariam,‡ and J. P. Cowin†

Environmental Molecular Sciences Laboratory, Pacific Northwest National Laboratory, Box 999 M/S K8-88, Richland, Washington 99352, and Varian Ion Implant Systems, 10130 SW Nimbus Avenue, Suite D7, Portland, Oregon 97223

Received: September 29, 1997; In Final Form: November 19, 1997

Nonstochiometric mixed oxides are often of interest for their novel catalytic or material properties yet are often difficult to synthesize in easily characterizable forms. We report on the use of low-temperature epitaxy of Ca and Mg under oxidizing conditions to yield mixed thin film oxides. Low-energy electron diffraction showed that the mixed oxides grew as single crystals over a wide range of compositions. We compare the water adsorption characteristics of the mixed oxide to that of CaO and MgO and find that the mixed oxide behavior is not a linear combination of the two pure oxide systems. The thermal stability of the mixed oxide film was checked by Auger electron ratios for an oxide−oxide "sandwich" after various "flash" anneals. This and water adsorption results suggest intimate atomic-scale mixing exists until flashed *above* 1100 K.

Introduction

1. Mixed Oxide Motivation. A mixed metal binary oxide is of composition $X_lY_mO_n$, where X and Y are two different metal cations. Mixed oxides can have various roles in environmental problems: This binary oxide could be a stoichiometric compound (the natural mineral spinel $MgAl_2O_4$), a dilute contaminant−host system (radioactive Cs in a sodium nitrate Hanford tank waste matrix), a nonstoichiometric mix ($Ca_xMg_{(1-x)}O$, a mixed oxide with novel chemistry), or the various glasses with dissolved contaminants for storage/disposal.

The difficulty in preparing good mixed oxide samples is greatly compounded when the mixed oxide has a large positive ΔH_{mix}. In this case, the mixed oxide will tend to be only available at exceedingly low concentrations or via some metastable preparation method, which typically has produced samples whose reactive sites are difficult to characterize. This paper explores the use of simultaneous vacuum co-epitaxy of a mixed oxide that is highly unstable but for which phase separation is very slow below 1100 K. This provides an excellent route for studying mixed oxides in general, and we expect the number of such studies will increase dramatically over the next few years.

The mixed Ca−Mg oxides we chose to study are definitely reluctant to mix: Mixing 1 mol of MgO and 1 mol of CaO requires about +47 kJ of free energy at 300 K.[1] Other studies show that Ca impurities in MgO surface segregate with a heat of segregation of about −50.3 kJ/mol.[2] They did observe one *encouraging* fact regarding making the mixed oxide: Rapid surface segregation occurred only for temperatures greater than or equal to 1300 K. So if one can metastably produce mixed Mg/Ca oxide at lower temperatures, the stoichiometry will likely remain unchanged below 1100 K or so.

CaO and MgO are potentially useful scrubbing agents for hot-bed destruction of chlorocarbons including carbon tetrachloride[3] and are used in many industrial processes. It was an interest of ours to determine whether we could make mixed Ca−Mg oxides in order to explore any novel chemistry it might have in such reactions. Mixed Ca−Mg oxides occur naturally in scrubbing applications where the common mineral dolomite ($CaMg(CO_3)_2$) is thermally decomposed prior to use: It produces some mixed $Ca_xMg_{(1-x)}O$ in addition to pure CaO and MgO.[1] Mixed Ca−Mg oxides have been made by rapid coprecipitation from solution and studied as to its methane oxidative coupling reactivity and selectivity.[4] Surface segregation of ppm Ca impurities in MgO crystals have been studied.[2,5,6] Recent work by Hellman and Hartford used cold co-epitaxy of Ca and Mg oxide to generate arbitrary lattice constants in subsequent epitaxy.[7] Their work, known to us only at the end of our study, helps us in interpreting our results.

2. Relevant Background. MgO single crystals are one of a few insulators that can be reasonably studied using many common ultrahigh-vacuum techniques, and much is known about it.[8,9] There has been much recent work in growing MgO in single-crystal thin films on Mo(100) substrates,[10,11] including recent work at this site.[3,9,12−14] The system is ordered and well-behaved, even though the MgO lattice is about 5% smaller than the Mo(100) substrate periodicity (after rotating the MgO azimuth 45°). CaO has been much less studied than MgO.[8,15,16] Only one ultrahigh-vacuum study of CaO exists to our knowledge.[15] Powders have been more studied, the work of Klabunde and co-workers being a good example.[16] Compared to MgO, CaO is a more reactive surface, with higher basicity, stronger water interactions, and greater likelihood of breaking bonds in adsorbates. CaO is roughly 7% too large to exactly lattice match Mo(100) for thin film growth. This is a similar magnitude of mismatch as for MgO, so perhaps the epitaxy would still work. And perhaps a 50%−50% mixture of Ca and Mg would work even better, as it would closely match the substrate periodicity. We will evaluate the structure and growth of the $Ca_xMg_{(1-x)}O$ oxide and examine the interaction with water, comparing it with that for MgO and CaO.

Experimental Section

The experiments were conducted in a ultrahigh-vacuum chamber with a base pressure of 2×10^{-10} to 6×10^{-10} Torr,

* Corresponding author.
† Pacific Northwest National Laboratory.
‡ Varian Ion Implant Systems.

S1089-5647(97)03169-6 CCC: $15.00
Published on Web 01/22/1998

pumped with a turbomolecular pump. The chamber had Auger electron spectroscopy (AES), low-energy electron diffraction (LEED), temperature-programmed desorption (TPD), and molecular beam dosing.[17] The Mo(001) sample was mounted to a pair of copper plates by a pair of tantalum wires (0.5 mm diameter), and the plates were in contact with a large copper piece cooled by a helium closed-cycle refrigerator. The sample could be heated either radiatively or by electron beam bombardment with filaments mounted in back of the crystal. The sample could be heated from 65 to 2000 K by this arrangement. Temperature was measured with type C (W−5% Re, W−26% Re) thermocouple material spot-welded to the edge of the crystal. Our particular thermocouple batch was later measured to be in fair agreement with published calibrations.[18]

The TPD experiments used a UTI mass spectrometer. The sample was radiatively heated for the TPD experiments. The high-purity calcium or magnesium dosing was achieved by a pair of line-of-sight evaporators which were carefully aligned so as to uniformly cover the sample. The flux of the evaporating metals was monitored with a line-of-sight mass spectrometer both before and after dosing. The thin film oxides were prepared by evaporating the metals onto a Mo(001) substrate in a background pressure of oxygen as discussed below.

The Mg and Ca sources could produce prodigious amounts of water, hydrogen, CO, and CO_2. Generally, we reduced spurious outgassing to a minimum by careful use, limiting exposure to air, and heating for extended periods of time before use. This problem was particularly serious for the Ca doser. If the Ca doser was used and then exposed to air, typically it became too contaminated with water for further use. If we had to vent the chamber, we simply cleaned the Ca doser and replaced the charge with fresh Ca metal. After outgassing during the chamber bake-out for about 2 days, we normally kept the Ca doser warm to limit buildup of serious water contamination. The Mg doser was much less troublesome. Working in this fashion, we routinely got water-free dosing of Mg or Ca, as evidenced by the lack of oxygen in AES for deposited pure or mixed metals.

Results and Discussion

1. Preparation of Mixed Ultrathin Oxide Films on Mo(001). *(a) Metal Deposition.* Pure metal deposition was studied, as the clear break from first monolayer to second monolayer in TPD's was used to characterize the metal doser flux and to help determine the oxide thicknesses (see below). Magnesium deposition was achieved by evaporation from magnesium ribbon wound around tantalum filaments that were resistively heated. Calcium deposition used a heated tantalum filament wound around a small piece of high-purity calcium (10 × 5 × 1 mm). Both sources suffered from changing Ta filament resistances due to melted Mg or Ca, and future studies will employ other arrangements. Both metal pieces were about 2 cm from the sample during deposition and were apertured so as to deposit mostly just on the sample. To examine the uniformity of dosing, some AES and TPD experiments were conducted after the dosing of the metals (without oxygen) onto Mo(001). AES showed that the film composition was uniform over the entire sample (since the spectra remained the same on moving the sample in both the horizontal and vertical directions by 6 mm).

TPD spectra for Mg adsorption on Mo(001) are shown in Figure 1. One peak was observed to desorb at about 730 K, while higher coverages desorbed near 540 K. Additionally, there is a small very high-temperature peak at a little over 1000 K, which is attributed to Mg adsorbed at surface defect sites.

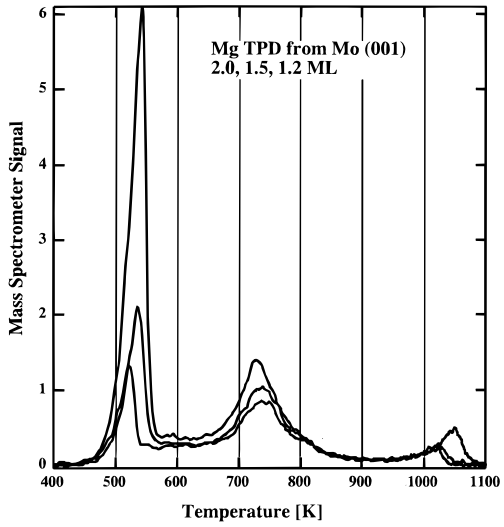

Figure 1. TPD of Mg on Mo(001).

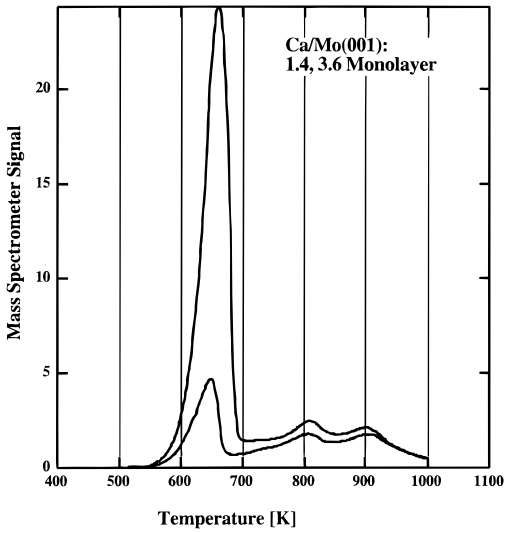

Figure 2. TPD of Ca on Mo(001).

Both the TPD and AES results were similar to others published.[10] Scanning tunneling microscopy and low-energy electron diffraction studies[10,12] both indicate that the first layer of Mg on Mo(100) grows in registry with the Mo(100) surface. This makes the integral of the coverage desorbed above about 600 K, when saturated, due to that from 1 monolayer of Mg (1.01×10^{15} Mg/cm^2).

The TPD spectra for various coverages of calcium on Mo(001) after growth at 300 K are shown in Figure 2. At low coverages, several desorption features are seen above 700 K. As the calcium coverage is increased, these features nearly saturate in height and shape. At higher calcium coverages, a desorption feature below 700 K is observed and is attributed to multilayer Ca growth. This desorption peak grows with increasing coverage without saturating. A natural log plot of the leading edge of the TPD curves versus reciprocal temperature for the coverages shown in Figure 1, and for higher yet coverages, shows zeroth-order desorption with an activation energy of about 160 kJ/mol and is in reasonable agreement with the reported heat of vaporization of 177.8 kJ/mol at 300 K.[19]

As the multilayer peak grows, the high-temperature features grow slightly in height and change shape slightly. We are not sure whether this a simple background growth in the Ca signal of the mass spectrometer or whether it reflects a real surface effect. As discussed below, this may be due to clustering or

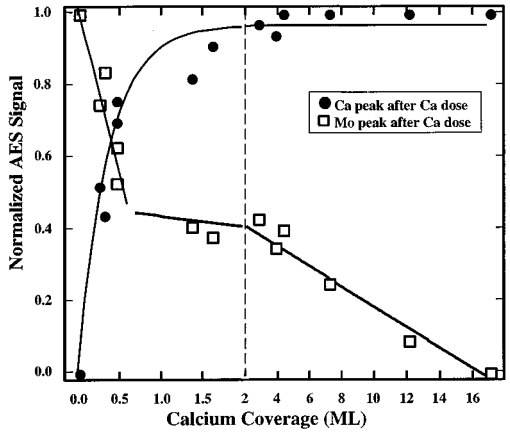

Figure 3. Auger peak signals as a function of increasing Ca dose. The circles show the increase in Ca peak signal with increasing Ca dose. The squares show the Mo peak signal decrease, which is linear in two regimes, <0.5 and >0.5 ML of Ca. (Note scale change at 2 ML.)

other nonplanar growth of the multilayer Ca. This complicates our assignment of what TPD integral constitutes a first complete monolayer. For the Ca epitaxy no scanning tunneling microscope work exists. Low-energy electron diffraction studies done by us show for Ca adsorption only diffuse scattering from Ca overlayers, indicating disordered overlayer growth. For simplicity, we attribute the integral from 700 K up for Ca deposition as due to a monolayer (8.6×10^{14} Ca/cm^2), the integral ideally taken for about 1.5 monolayer exposure.

Figure 3 shows the AES results obtained during the deposition of calcium metal on the Mo substrate, plotted versus the calcium coverage from TPD. Calcium exhibits a prominent Auger peak at 291 eV, due to *LMM* transitions, while Mo(001) shows characteristic Auger peaks at 186 and 221 eV. The intensities of the characteristic AES features (291 eV peak for calcium and 186 eV peak for molybdenum) are plotted in Figure 3. The squares refer to the peak-to-peak intensity of the 186 eV molybdenum feature normalized to pure molybdenum signal, while the circles refer to the 291 eV calcium feature, normalized to pure calcium (infinite thickness limit).

From an inspection of Figure 3, it can be seen that the molybdenum features vanish only at very high coverages during the growth of metallic calcium on Mo(001) and show roughly linear falloff rather than a simple exponential. This behavior suggests that calcium grows as three-dimensional islands after the completion of the first layer.[20] The absence of any ordered LEED patterns for multilayer calcium also supports this growth scheme. In contrast, magnesium grows in a layer-by-layer fashion on Mo(001) for the first four layers, after which island growth occurs. The layer-by-layer growth proceeds first with face-centered-cubic stacking and then hexagonal closed-packed stacking, as seen by both LEED and scanning tunneling microscopy.[10,12] The differences between growth modes of magnesium and calcium can be understood in terms of differences in their lattice match with the Mo(001) substrate. Magnesium can grow on Mo(001)with a lattice mismatch of +2%, while calcium is much larger and has a lattice mismatch of more than +20%. Thus, the Mo(001) provides a reasonable template for the growth of face-centered-cubic magnesium monolayers but not for the growth of calcium.

(b) MgO/CaO Deposition and Characterization. The method used in the preparation of the oxide films was similar to the one developed by Wu and co-workers.[10] During metal evaporation, we dosed the sample with two effusive oxygen dosers,

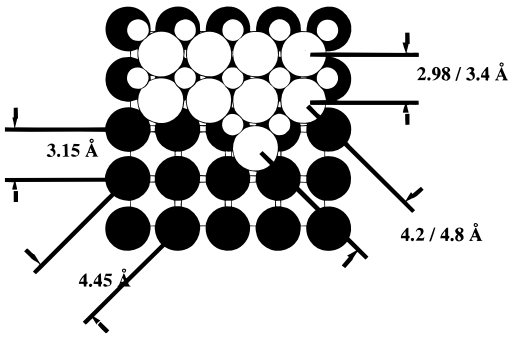

Figure 4. MgO or CaO metal oxide overlayer structure on Mo(001). The darkest circles represent the Mo(001) surface, large light circles O^{2-}, and small circles Mg^{2+}/Ca^{2+}.

1.1 cm from the sample and 70° from its normal, to establish a total main chamber pressure rise of about 5×10^{-8} Torr. Assuming the main chamber pumping speed is 400 L/s, an incident angle of 70°, and that the sample subtends only a small fraction of the total solid angle of the beam, this gives an approximate local oxygen fluence corresponding to a local equivalent pressure of 2×10^{-7} Torr. The metal dosers dosed at rates of 0.5−1.0 monolayer/min. For much lower pressures, the oxidation was incomplete. For much higher pressures, it gave poor LEED patterns (this was even more true for MgO thin films), perhaps due to too much oxidation of the Mo substrate. For MgO, after growth near 320 K temperature, the sample was flashed to 1100 K to anneal the oxide. This gave LEED patterns that had well-defined spots, though rather broad: For 85 eV primary energy, the spot fwhm's were about $^1/_8$ of the spacing between spots. The bare Mo(001) surface spots were quite sharp, with fwhm's about 0.04 of the spot separation at the same condition. The (100) face of the Mo body-centered-cubic lattice has a square periodicity, as shown in Figure 4. The (100) face-centered-cubic rock salt structure of MgO and CaO also has a square structure, either with a centered atom if the cubic lattice is chosen or rotated 45° from this, a simple square. The latter nearly matches the Mo(100) face, as indicated in Figure 4. An epitaxial layer of MgO or CaO will line up as shown. The Mo (1 × 1) LEED pattern matches the c(1 × 1) of the oxide surface. This creates some ambigiuty for labeling diffraction features. We shall refer to the observed diffraction spots as (1 × 1). Some additional details on CaO growth are given below. Most details on MgO, and more on CaO, can be found in ref 13.

The thickness of the film was fundamentally determined by dosing under the same conditions as that giving a known coverage (via TPD) of unoxidized Ca on Mo. Under some conditions in this experiment, we correlated the AES signals with the pure metal TPD data to inform us about the CaO coverage on Mo. Figure 5 shows the results of AES obtained during the deposition of calcium oxide, correlated with coverage. As in Figure 3, the squares refer to the peak-to-peak intensity of the 186 eV molybdenum feature normalized to that seen for pure molybdenum, while the circles refer to the 291 eV calcium feature, normalized to pure CaO signal. The pure CaO signal was obtained in the limit of very thick CaO films, where no Mo peaks were visible.

The coverages for this figure were determined using identical Ca metal exposures (without oxygen) whose coverage amounts could be obtained from TPD integrals. In this, we assume that 1 ML coverage of Ca metal gives 1 ML coverage of CaO. This is a reasonable assumption as the Ca atoms would occupy the same sites on the Mo substrate in either a pure Ca(100) plane

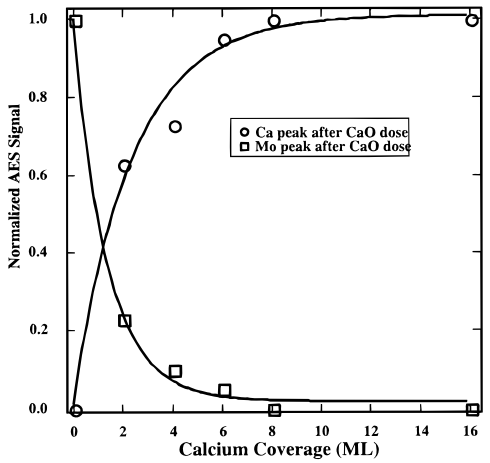

Figure 5. Auger peak signals as a function of increasing CaO dose. The circles show an increase in Ca peak signal with increasing CaO coverage. The squares show the decrease in Mo peak signal with increasing CaO coverage.

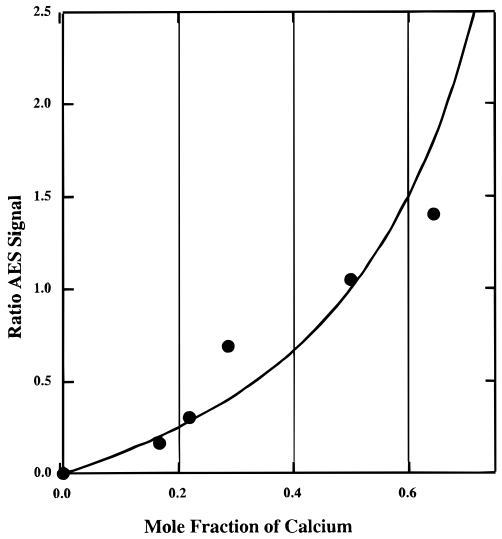

Figure 6. AES ratios of calcium to magnesium as a function of thin oxide film composition. The AES ratio is the ratio of peak-to-peak intensities ($[I_{Ca-291}/I^{o}_{Ca-291}]/[I_{Mg-32}/I^{o}_{Mg-32}]$), where I^{o} stands for the intensity of seen for the pure oxides (i.e., very thick films). This is plotted versus X, the mole fraction of Ca in the film. The smooth curve is $X/(1 - X)$.

or the CaO (100) plane. The only caveat is that the pure Ca thin film would be under more compressive strain than the oxide. We also assume that the metal atom sticking probability is constant. We have good reason, in the pure metal deposition case, to believe that the sticking probablility is unity, given how very much larger the binding energy is compared to the incident atom kinetic energy, how difficult any configurational barrier to adsorption would be to imagine, and how much higher is the desorption temperature than the deposition temperature. For the metal oxide surface, it is *possible* that the sticking probability is significantly less than one. We did not directly measure this sticking probability, though the general strong shielding seen for Mo substrate AES signals versus nominal Ca or Mg oxide thicknesses (Figure 5) indicates that the sticking probability on the oxide cannot be small. In the case of the pure MgO oxide, STM studies[12] allow us to count the number of monolayers typically present under dosing for both pure Mg and MgO. That data show that the sticking probability did not vary more than 25% or so from a single constant value during growth of pure metal or oxide.

We hoped to produce layer-by-layer growth of these oxides. If the oxide grows this way, we would expect to see a strong, continuous attenuation of the substrate AES signal as the overlayer thickness grows, down to essentually zero substrate signal. If there were some substrate AES signal that persists for high overlayer thickness, this is a good indication that the overlayer is not "wetting" the substrate and is leaving very thin (or bare) spots. With MgO, where we compared the STM images versus growth conditions with AES data, the STM showed layer-by-layer growth, and the AES signal correspondingly showed rapid, complete attenuation of substrate signal with increasing oxide thickness. At other growth conditions (very high temperature), considerable non-layer-by-layer growth was observed, with bare spots down to the substrate, coexisting with a persistent substrate signal in the AES signal.[12]

The AES data shown in Figure 5 clearly suggest that CaO grows in a simple layer-by-layer fashion: One can see the Ca feature increases and the Mo feature correspondingly decreases with increasing CaO coverage. The Mo peak is essentially gone after 6−8 monolayers of CaO coverage and shows roughly exponential falloff, as would be expected for simple attenuation by a uniform smooth film. The CaO film seems to do a better job of covering over the Mo substrate than the pure Ca metal film did. Thus, the trend seen with pure Ca metal deposition favoring three-dimensional island growth does not occur when growing the CaO film.

The stoichiometry of calcium oxide was verified by ensuring that the oxygen AES peak at 505 eV did not increase and the Ca/O AES ratio remained constant on subsequent attempts at oxidation. In addition, (1 × 1) LEED patterns were observed for film thickness greater than 3−4 ML. The LEED spots were generally broader than for MgO thin films, indicative of the films being made up of small domains of CaO(001). Thinner films of CaO gave only a bright, diffuse background.

(c) Mixed Oxide Deposition. Mixed films of magnesium and calcium oxides were prepared by depositing the two metals simultaneously onto the Mo(001) 320 K substrate with oxygen dosing, again at a local pressure of about 2×10^{-7} Torr of O_2 and at metal deposition rates of 0.5−2 ML/s. The composition of the mixed oxide film was controlled by varying the relative evaporation flux from the metal sources. Since MgO(001) is 5% smaller than Mo(001) and CaO(001) is 7% larger than Mo(001) (see Figure 4), a good lattice match is expected for a mixture of calcium and magnesium oxide. The whole range of compositions was examined, from $x = 0$ to 1 for $Ca_xMg_{(1-x)}O$. After growth near room temperature, the sample was typically flash-annealed at 1100 K.

The AES peaks for Ca and Mg in the mixed oxide appear at the same energies as seen in the pure MgO and CaO (and different than for the unoxidized metals). Figure 6 shows the AES ratios of calcium to magnesium as a function of thin film composition. The AES ratio is obtained by utilizing the ratio of peak-to-peak intensities ($[I_{Ca-291}/I^{o}_{Ca-291}]/[I_{Mg-32}/I^{o}_{Mg-32}]$), where I^{o} stands for the peak intensity for the pure oxide case. Such a use of relative intensities allows the various instrumental contributions to sensitivity to be reduced to a single factor, under the assumption that the electron mean free paths for the various transitions are not sensitive to the composition of the oxide. The mole fractions were obtained by using TPD integrals of unoxidized mixed metal films, grown under the same conditions just before or after the Auger data were taken for the mixed oxide films. We would expect the plot in Figure 6 to vary approximately as $X/(1 - X)$ where X is the Ca mole fraction. The relationship depicted in this figure then provides a

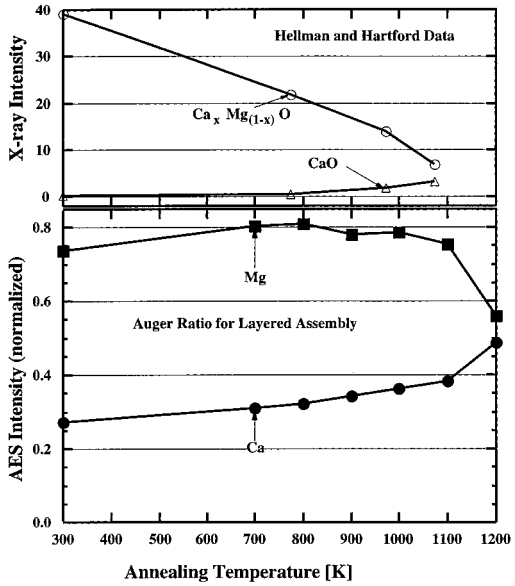

Figure 7. Thermal unmixing of mixed Ca−Mg oxide. The upper pair of curves is from the X-ray diffraction data of Hellman and Hartman.[16] They show the decrease in the mixed oxide diffraction intensity as a function of the 1 h anneal peak temperature. The lower pair of curves show the intensity of the magnesium and calcium AES peaks plotted as a function of flash-anneal temperature. The squares and circles correspond to the normalized AES intensity of the characteristic Mg and Ca peaks, respectively.

convenient way to determine the respective amounts of Ca and Mg in the mixed oxide.

The equilibrium solid solubility of MgO in CaO and CaO in MgO is very small at the temperatures used in our work, as the critical solubility temperature for this system is 2640 K. In light of this thermodynamic tendency for the $Ca_xMg_{(1-x)}O$ to phase separate, it is important to examine the stability of this system. One of the parameters that governs the stability of the films is the segregation or diffusion of the cations. To examine the diffusivity of ions, a thick CaO layer (10 ML) was sandwiched between a thin layer of MgO (2 ML) and the Mo-(001) substrate. The intensity of the magnesium and calcium AES peaks were measured initially and then after various sequential flash anneals. For the anneals the sample was heated at roughly 25 K/s to the target peak temperature, and then the heating was stopped. Cooling occurred initially at about 15 K/s. The resulting AES intensities are plotted as a function of peak annealing temperature in Figure 7 (the lower pair of curves). The squares and circles correspond to the AES intensity of the characteristic Mg and Ca peaks, respectively. From an inspection of the curves, it is clear that the Ca/Mg ratio increases only at flash temperatures above 1100 K. There is no significant diffusion of calcium occurring until the sample temperature is above 1100 K. This result is in reasonable agreement with studies of calcium segregation to MgO(001) surfaces utilizing ion scattering spectroscopy (ISS),[2,5] AES,[2] RHEED, and REELS.[6] The AES experiment shown in Figure 7, although not exploring the structure or composition of the mixed oxide directly, provides some insight into the stability of the film. The low mobility observed for the cations suggests that negligible unmixing of a mixed layer occurs at temperatures of interest. The deposition of the mixed oxide thus results in the formation of kinetically limited metastable films.

These findings are consistent with recent studies by Hellman et al.[7] on the growth of metastable solution of CaO/MgO on MgO(001) by molecular beam epitaxy. The upper pair of curves in Figure 7 are derived from their published X-ray diffraction

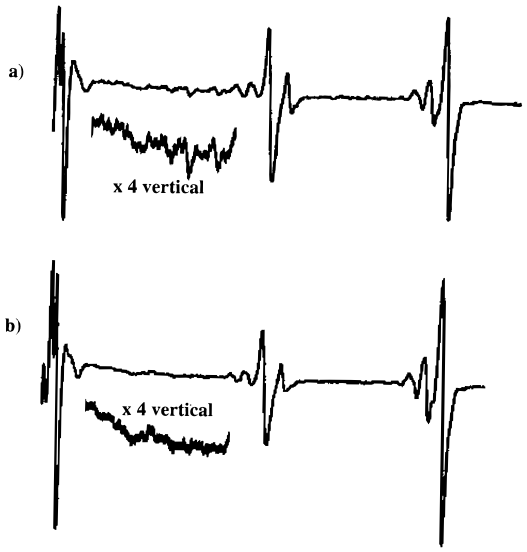

Figure 8. Comparison of Auger spectra for the mixed Ca/Mg oxide film: (a) 17 ML thickness of $Ca_{0.3}Mg_{0.7}O$, grown a few monolayers at a time and annealed prior to each additional amount grown; (b) 15 ML thickness of $Ca_{0.2}Mg_{0.8}O$, grown all at once, no anneal.

data. In their paper, the $Ca_xMg_{(1-x)}O$ films (roughly 150 nm thick) were grown at 300 °C, and their structural properties were examined with RHEED and X-ray diffraction, while the composition was examined with Rutherford backscattering spectroscopy (RBS). These studies suggests that the lattice spacing changes monotonically (Vegard's law behavior) from that of pure CaO to that of pure MgO as the composition is varied. Figure 7 shows the decrease in the mixed oxide diffraction intensity for a 1.2 to 1 ratio Ca to Mg oxide film, as the sample was subjected to higher temperature 1 h anneals. This decrease continues for some time before a corresponding increase in the pure CaO signal becomes substantial, at around 1000 K.

The morphology of the films we grew were dependent on growth conditions and composition. Figure 8 shows the AES of very similar mixed oxide films grown under two different conditions. Trace a is from a 17 ML film grown in steps; i.e., a few monolayers were deposited and then annealed to 1100 K, at which point more was deposited and annealed. This step annealing was continued until the final thickness was achieved. The molybdenum peaks, though small, are still apparent, indicating bare or very thinly covered patches in the film. Trace b is from a 15 ML film grown all at once, with no annealing (data are similar to that for a single 1100 K flash anneal). A comparison of the blown-up regions of the curves clearly shows that the Mo features in trace a do not exist in trace b. We conclude that this method of growth was more effective in producing flatter, more homogeneous films.

Differences due to composition were observed with LEED. For MgO-rich mixed oxide films ($Ca_xMg_{(1-x)}O$, $x < 0.3$), (1 × 1) LEED patterns were observed for all coverages. For roughly evenly mixed oxide films to CaO-rich films, a (1 × 1) LEED pattern was exhibited only for thick films (greater than 3−5 ML). The thinner CaO-rich films showed no diffraction spots but only a bright, diffuse background, similar to the thin film pure calcium oxide. In all cases, these thicker films often showed good LEED patterns even without flash annealing. The spot size of the LEED patterns varied somewhat with condition but were not greatly different and tended, for 85 eV primary energy, to show spot fwhm's that were about $^1/_6$ of the spacing between spots. One might have expected a "magic ratio" to be

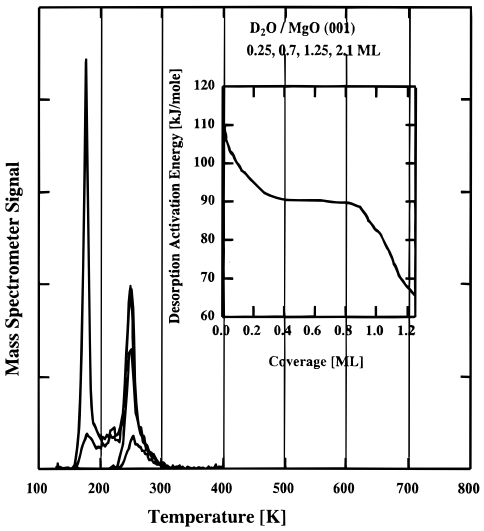

Figure 9. TPD of water adsorbed on MgO(001). Oxide film is about 30 monolayers thick. Water coverages are 0.25, 0.7, 1.25, and 2.1 ML. The inset of the figure shows the activation energy calculated for the 1.25 ML D_2O curve assuming a preexponential factor of 10^{-14}/s.

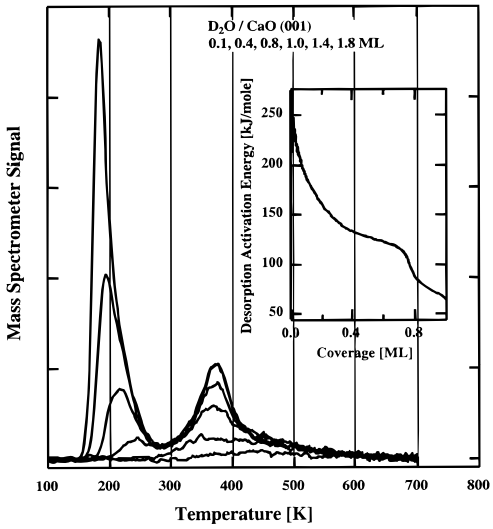

Figure 10. TPD of water adsorbed on CaO(001). Oxide film is about 25 monolayers thick. Water coverages are 0.1, 0.4, 0.8, 1.0, 1.4, and 1.8 ML. The inset shows the activation energy for the 1 ML D_2O curve assuming a preexponential factor of 10^{-14}/s.

observed in LEED, where the lattice parameters of the mixed oxide would perfectly match the Mo(001) substrate to produce a strain-free mixed oxide film. This would occur at about a $Ca_{0.4}Mg_{0.6}O$. We had hoped to see *very* sharp LEED spots near this ratio. We did not. However, as we did not explore a wide range of preparation and annealing conditions, perhaps this magic ratio might yet give a perfect lattice match.

(d) Coverage Determination. In the course of the experiments, it was troublesome to determine coverages accurately and to maintain truly constant dosing conditions. This was especially true for the oxide films and mixed oxide films. The line-of-site mass spectrometer sensing the dosing flux was too far away and had interferences with chamber mass 40 (Ar) backgrounds. Dosing reproducibility was adequate (typically) to allow thin film metals to be grown and their TPD examined, to calibrate the doser that day for each metal deposited. In some cases this was how coverages were measured. In other cases, the AES calibration curves in Figures 3, 5, and 6 were used to estimate the coverages, sometimes in combination with metal TPD's. It is likely that 25% errors in coverages still persist. Most of the effects we see are not strongly coverage dependent, and when some are, we are clearly in the asymptotic region of "high coverage" (>15 ML).

2. Water Adsorption on the Oxide Films. *(a) Water Adsorption on Pure MgO and Pure CaO.* The chemistry of these oxide surfaces was examined with temperature-programmed desorption of water. D_2O was used in order to avoid interference from the background water present in the chamber. Water coverages are reported based on desorbed integrals, but generally sticking probabilities are nearly unity for these systems. The TPD's done for water were often done on surfaces that had been previously used for other water TPD's. However, we noted no differences for either pure or mixed oxide surfaces between those that had no previous water TPD's or many, despite temperature flashes to ~800 K between each TPD. This is in accord with the data of Figure 7. The TPD of D_2O from MgO is shown in Figure 9 and from CaO in Figure 10. The metal oxide films were thick enough to exhibit the sharp D_2O TPD features as discussed below.

The coverage-dependent TPD spectra presented in Figure 9 are typical of water adsorbed on clean ordered MgO(001) and are similar to those obtained for both thin films of MgO[11] and bulk single crystals of MgO(001)[9] in UHV. The inset of the figure shows the activation energy calculated for the 1.25 ML D_2O curve, assuming a preexponential factor of 10^{-14}/s. There was no desorption of chemical species other than the parent D_2O molecules. The desorption features seen above 200 K can be attributed to water chemisorbed on MgO, while the lower temperature features are due to desorption of multilayer ice. The total desorption under the sharp TPD peak at 250 K is assumed to be 1 ML for the calibration of water coverage and is attributed to water desorption from (001) terraces. The sticking probability of water on MgO was found to be constant and was assumed to be unity. Stirniman and co-workers[9] have suggested that the broad desorption features between the sharp 250 K peak and the low-temperature ice peak are due to a partial second layer which begins to force the adsorbed first monolayer of water, which is in registry with the square MgO lattice, to adopt the hexagonal structure of a multilayer ice film. The high-temperature tail of the 250 K monolayer peak is attributed to water adsorbed on the extended defects (such as ledge and kink defects), the details of which have been published elsewhere.[13] The desorption energies of water from the defect sites is 110 kJ/mol, while the desorption from terrace sites have a smaller value of 90 kJ/mol.

The TPD of water adsorbed on CaO(001) is shown in Figure 10, the inset showing the activation energy for the 1 ML curve, assuming a preexponential factor of 10^{-14}/s. The spectra consist of three main features. A desorption peak is seen at roughly 375 K. In addition to this is a high-temperature tail extending up to 600 K. A third desorption feature appears at coverages roughly greater than 0.6 ML, while the higher temperature features are still filling in. It is initially seen with a peak temperature of 250 K (for 0.8 ML of D_2O), shifts to lower temperatures with increasing water coverages, and merges into the multilayer ice desorption curves. Although these TPD features do not exhibit first-order behavior, an analysis assuming first-order kinetics can yield interesting qualitative insights into the energetics of water adsorption on alkaline earth oxides.

A comparison of Figures 9 and 10 clearly shows that water is more strongly adsorbed on CaO than MgO. At least part of the water desorbs with a peak temperature of 350 K on CaO as compared to the 250 K desorption peaks seen on MgO, and this corresponds to a difference of 25−50 kJ/mol in desorption

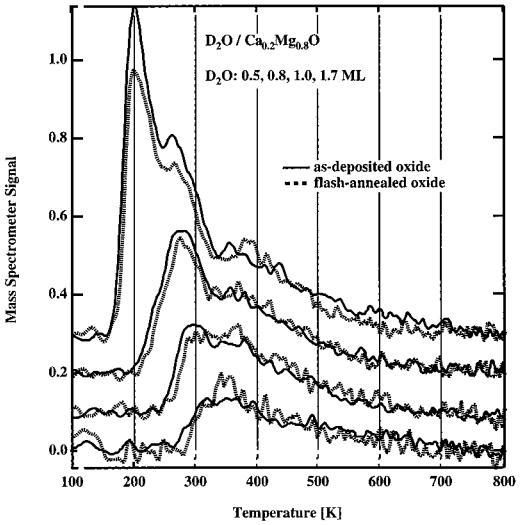

Figure 11. TPD of D_2O on ($Ca_{0.2}Mg_{0.8}O$). TPD of water from mixed Ca/Mg oxide, for both a nonannealed and flash-annealed film, about 15 monolayers thick. Water coverages are 0.5, 0.8, 1.0, and 1.7 ML.

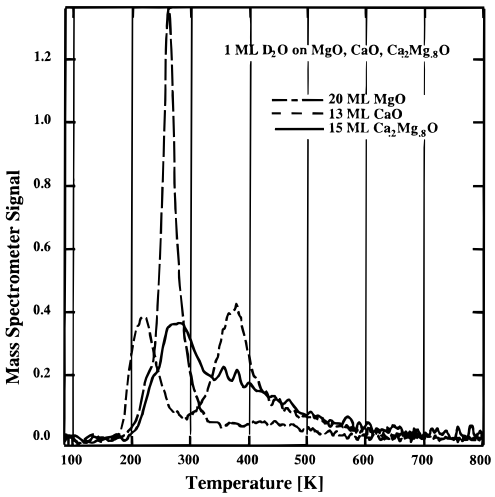

Figure 12. Comparisons of TPD's of 1 ML of D_2O on MgO, CaO, and $Ca_{0.2}Mg_{0.8}O$.

energy for water adsorption on these oxides. We also have conducted TPD experiments on isotopically labeled thin oxide films ($Mg^{18}O$ and $Ca^{18}O$) which is reported elsewhere.[13] These results showed that there is significant exchange of oxygen between the adsorbed water and the CaO lattice. This certainly means that water at some point dissociates. No scrambling occurred in the case of water on MgO, and recent results from Goodman's group[21] give strong evidence for water adsorption on MgO being nondissociative.

The low-temperature desorption peak in Figure 10 is distinct from a multilayer peak, although they eventually merge together. This peak showed no isotopic exchange of oxygen for this peak in our $Ca^{18}O$ TPD, although this alone does not indicate whether this water adsorbed dissociatively or molecularly. The higher temperature peak does show oxygen exchange with the lattice, which certainly indicates that at least sometimes the water must dissociate. It can be seen that this low-temperature peak shifts to even lower temperatures with increasing coverage. This behavior may be due to dipole−dipole repulsion between molecularly adsorbed water. This may indicate that the CaO−water interaction is strong enough to orient all the water molecules the same way, rather than permit growth of the common, hydrogen-bonded, ice-like "bilayer". Evidence of a diffusion barrier between the low- and high-temperature desorption states is seen, as both the low- and high-temperature desorption peaks fill simultaneously with increasing water coverage.

The adsorption characteristics of water on magnesium and calcium oxides are in agreement with the expectations of chemical reactivity, the conventional wisdom suggesting that basicity of the oxides increases as the cation size increases. Theoretical studies suggest that differences between these oxides arise primarily from the differences in the ability to protonate the oxygen anion rather than the differences in hydroxylating the cations.[22] These studies also have attributed this phenomenon to an increase in the ionicity (as quantified from the oxygen charge) with increase in cation size. The conventional pictures depict alkaline earth oxides as perfectly ionic materials.

(b) Water Adsorption on Mixed Mg/Ca Oxides. The TPD's of D_2O on a mixed calcium/magnesium oxide film ($Ca_{0.2}Mg_{0.8}O$) grown at 320 K are shown in Figure 11. A set of TPD's were done on the unannealed film, after which it was flash-annealed to 1100 K. Water TPD from that surface was then repeated, and the results from both the unannealed and flash-annealed films appear in Figure 11. They are very similar. The monolayer peak saturates at about 275 K, with a broad higher temperature tail. While the various desorption features are reminiscent of either pure CaO or pure MgO, the overall TPD behavior is *not* a linear combination of desorption from these oxides. This is more clear in Figure 12, which shows 1 ML D_2O desorption from either of the pure oxides and from the mixed oxide. If the mixed oxide had managed to separate into small domains of pure CaO and pure MgO, a linear combination of the two would have resulted. Our results suggest the mixing is intimate and is consistent with our AES data and data of other groups[2,5−7] that show that mobility is limited at low temperatures. We envision that Mg and Ca should simply substitute for each other in a slightly defected rock salt lattice. With very limited mobility, nearly random occupation may be the rule. An additional unique feature for the mixed oxide is the extensive high-temperature tail seen in the water TPD. This suggests that despite having LEED patterns showing similar long-range order for the mixed versus the pure oxide, the mixed oxide would appear to have a great many more defects present than either pure oxide. This would be a likely result of fairly random substitutional defects, where size and chemical differences should create many unique sites, with more defects.

A possibility other than intimate mixing could be argued: Perhaps extremely small domains of pure CaO and MgO form, which are also extremely highly defected. The small mobility seen in the annealing studies (Figure 7) argues against this. Additionally, it is difficult to see how partial separation would yield LEED patterns as good as we saw. A chemical test is also possible. Figure 11 shows that the water TPD changes little with or without the flash anneal. The LEED pattern was fairly sharp in both instances, indicating reasonable long-range ordering. It is extremely unlikely that at the growth temperature of 320 K that the flash-annealed mixed oxide could "unmix". That its water chemistry is unchanged after the flash anneal is perhaps the most compelling evidence that the mixed oxide formed from co-epitaxy of Ca and Mg is *intimately mixed* at the atomic level.

Conclusions

We have demonstrated the low-temperature stability of the mixed metal oxide films $Ca_xMg_{(1-x)}O$. The evaporative deposition we used yielded ordered *thick* films in the entire composi-

tion range and ordered Mg-rich mixed oxide films for *any* thickness. The films had a demonstrable uniform thickness, growing in approximately layer-by-layer fashion as shown by Auger spectroscopy.

The as-deposited compositionally mixed films were indeed intimately mixed. We were able to show that significant diffusion of the metal species does not occur unless the temperature of the film is flashed to greater than 1100 K. This is in qualitative agreement with previous work[7] done on this system, which had indicated that 1 h anneals did not greatly unmix the oxide films until temperatures were substantially elevated (∼1000 K). As pointed out in that work, the epitaxial quenching is quite successful in producing kinetically limited metastable films which are well-mixed and remain so.

Finally, for at least one composition of mixed $Ca_xMg_{(1-x)}O$ film, the mixed oxide seems to possess distinct chemical properties from its constituent pure oxides, at least in regards to its behavior with adsorbed water. The TPD of D_2O on the mixed oxide film is not a linear combination of desorption from pure CaO and pure MgO. It still remains to further investigate the chemical/catalytic properties of this and other compositional mixes of $Ca_xMg_{(1-x)}O$.

Acknowledgment. The Environmental Molecular Sciences Laboratory is a collaborative users' facility of the Department of Energy [D.O.E.] Office of Health and Environmental Research. Funded by Office of Chemical Sciences, D.O.E. Pacific Northwest National Laboratory is operated by Battelle Memorial Institute for the D.O.E. under Contract DE-AC06-76L0-1830.

References and Notes

(1) Spinolo, G.; Anselmi-Tamburini, U. *J. Phys. Chem.* **1989**, *93*, 6837.
(2) McCune, R. C.; Wynblatt, P. *J. Am. Ceram. Soc.* **1983**, *66*, 111.
(3) Zhou, X.-L.; Cowin, J. P. *J. Phys. Chem.* **1996**, *100*, 1055.
(4) Philipp, R.; Omata, K.; Aoki, A.; Fujimoto, K. *J. Catal.* **1992**, *134*, 422.
(5) Souda, R.; Aizawa, T.; Ishizawa, Y.; Oshima, C. *J. Vac. Sci. Technol. A* **1990**, *8*, 3218.
(6) GajdardziskaJosifovska, M.; Crozier, P. A.; McCartney, M. R. *Surf. Sci.* **1993**, *284*, 186. Crozier, P. A.; GajdardziskaJosifovska, M. *Ultramicroscopy* **1993**, *48*, 63.
(7) Hellman, E. S.; Hartford, E. H., Jr. *Appl. Phys. Lett.* **1994**, *64*, 1341.
(8) Henrich, V. E.; Cox, P. A. *The Surface Science of Metal Oxides*; Cambridge University Press: Cambridge, 1994.
(9) Stirniman, M. J.; Huang, C.; Smith, R. S.; Joyce, S. A.; Kay, B. D. *J. Chem. Phys.* **1996**, *105*, 1295.
(10) Wu, M. C.; Corneille, J. S.; He, J. W.; Estrada, C. A.; Goodman, D. W. *J. Vac. Sci. Technol. A* **1992**, *10*, 1467.
(11) Wu, M. C.; Estrada, C. A.; Corneille, J. S.; Goodman, D. W. *J. Chem. Phys.* **1992**, *96*, 3892. Wu, M. C.; Goodman, D. W. *Catal. Lett.* **1992**, *15*, 108.
(12) Gallagher, M. C.; FyField, M. S.; Joyce, S. A. *Surf. Sci.* **1995**, *339*, L909 and to be published.
(13) Kizhakevariam, N.; Iedema, M. J.; Gallagher, M. C.; Joyce, S. A.; Cowin, J. P. Manuscript in preparation.
(14) (a) Chambers, S. A.; Tran, T. T.; Hileman T. A. *Mater. Res.* **1994**, *9*, 2944. (b) Chambers, S. A.; Gao, Y.; Liang, Y. *Surf. Sci.* **1995**, *339*, 297.
(15) Lee, V. C.; Montano, P. A.; Cook, J. M. *Surf. Sci.* **1984**, *143*, 423.
(16) Koper, O.; Li, X.; Klabunde, K. J. *Chem. Mater.* **1993**, *5*, 500.
(17) Marsh, E. P.; Tabares, F. L.; Schneider, M. R.; Gilton, T. L.; Meier, W.; Cowin, J. P. *J. Chem. Phys.* **1990**, *92*, 2004.
(18) Mitchell, W. J.; Xie, J.; Weinberg, W. H. *J. Vac. Sci. Technol. A* **1993**, *11*, 3133. Sandstrom, D. R.; Withrow, S. P. *J. Vac. Sci. Technol.* **1977**, *14*, 748.
(19) Lide, D. R., Ed. *Handbook of Chemistry and Physics*, 74th ed.; CRC Press: Boca Raton, FL, 1993; p 5-1.
(20) Argile C.; Rhead, G. E. *Surf. Sci. Rep.* **1989**, *10*, 277.
(21) Xu, C.; Goodman, D. W. *Chem. Phys. Lett.* **1997**, *265*, 341.
(22) Goniakowski, J.; BouetteRusso, S.; Noguera, C. *Surf. Sci.* **1993**, *284*, 315. Goniakowski, J.; Noguera, C. *Surf. Sci.* **1995**, *330*, 337.